

Muonic vs electronic dark forces: a complete EFT treatment for atomic spectroscopy

Claudia Frugiuele,^a and Clara Peset^b

^a*INFN, Sezione di Milano,
Via Celoria 16,
I-20133 Milano, Italy*

^b*Technische Universität München,
Physik Department,
James-Franck-Straße 1,
D-85748 Garching, Germany*

E-mail: claudia.frugiuele@cern.ch, clara.peset@tum.de

ABSTRACT: Precision atomic spectroscopy provides a solid model independent bound on the existence of new dark forces among the atomic constituents. We focus on the keV-GeV region investigating the sensitivity to such dark sectors of the recent measurements on muonic atoms at PSI. To this end we develop for the first time, the effective field theory that describes the leading effect of a new (pseudo-)vector or a (pseudo-)scalar particle of any mass at atomic energies. We identify in the Lamb Shift measurement in muonic deuterium (μD) and the $2s$ Hyperfine Splitting (HFS) in muonic hydrogen (μH) the most promising measurements to probe respectively spin-independent and spin-dependent new forces. Furthermore, we evaluate the expression of the vector force HFS finding that a future measurement of the $2s$ HFS in regular hydrogen could provide the strongest atomic bound for such a force for masses above 100 MeV.

TUM-HEP-1354/21

Contents

1	Introduction	1
2	Testing dark forces via Lamb shift measurements	2
3	Testing dark forces via Hyperfine splitting measurements	4
4	Testing dark forces via $1s - 2s$ splitting measurements	6
5	Probing dark forces via laser muonic spectroscopy	7
5.1	Spin-independent dark forces	11
5.2	Spin-dependent dark forces	15
6	Conclusions	16
A	The EFT for new particle interactions	17
A.1	The nonrelativistic EFT	17
A.2	The potential NREFT	19
B	Expectation values	21

1 Introduction

There have been substantial advances in controlling matter and light in the last 20 years, creating new opportunities in atomic, molecular and optical physics such as novel probes of physics beyond the Standard Model (BSM) [1–13]. This has come at the ideal time for particle physics. Indeed, traditional approaches to BSM physics have been deeply challenged by the results of new physics searches carried out at the Large Hadron Collider (LHC) [14], and by the absence of a positive signal at dark matter (DM) direct detection experiments. As a reaction, new ideas have blossomed showing how BSM compelling inquiries such as the existence of DM [15] or the hierarchy problem [16] could be connected to the existence of low mass dark sectors, very weakly coupled to the visible sector. Since high energy colliders have limited sensitivity to such dark particles, the main players in this quest are experiments at the intensity or precision frontier [17].

New forces between the dark and the visible sectors might modify atomic energy levels and thus could be detected via precision spectroscopy. For simple atoms such as atoms with few electrons or exotic hydrogen-like atoms, one can rely on the comparable precision

between the theoretical calculations and the experimental measurements such that the effect of dark forces can be bounded by comparing the experimental and theoretical errors [3–7]. For atoms with many electrons, a different strategy [11–13] should be followed due to the limited precision of the theoretical calculations.

In this work, we will examine the sensitivity to dark forces of muonic atoms, that is hydrogen-like atomic bound systems formed by a negative muon and a nucleus. These atoms are smaller than standard atoms by a factor of $(m_e/m_\mu)^3 \sim 8 \cdot 10^6$, which makes them potentially more sensitive to intermediate scale new forces, i.e. mediated by particles with masses in the MeV-GeV range. Such forces are typically mediated by particles with masses close to the reduced mass of the system $\sim m_\mu$ which typically produce a contact interaction rather than a potential-like exchange at atomic-like energies. We deal with this issue by developing, for the first time, an effective field theory (EFT) that accounts for the leading effect of mediators in any mass range. We also compute the one-loop matching coefficients that some of the leading effects which we study here require. The paper is organized as follows. In Section 2, we present the contribution given by new force carriers to the Lamb shift (LS) of a generic hydrogen-like atom. In Section 3, we consider the HFS not only for spin-dependent, but also for spin-independent forces mediated by a new vector boson. In Section 4, we provide expressions for $1s - 2s$ splittings for atoms with components of equal and different masses. In Section 5, we explore the sensitivity of the PSI measurements on muonic atoms to spin-independent and spin-dependent dark forces. We also update the bound from the Lamb shift measurement in regular hydrogen considering the recent experimental result [18] and the new determination of the proton charge radius.

2 Testing dark forces via Lamb shift measurements

We consider new physics forces mediated by an axial-vector (A), vector (V), scalar (S) or pseudo-scalar (P) particle of mass m_ϕ that couples to the Standard Model fermions as

$$\mathcal{L}_V = g_V \bar{\psi} \not{V} \psi, \quad \mathcal{L}_A = g_A \bar{\psi} \not{A} \gamma^5 \psi, \quad \mathcal{L}_S = g_S \bar{\psi} S \psi, \quad \mathcal{L}_P = i g_P \bar{\psi} P \gamma^5 \psi. \quad (2.1)$$

We take an EFT perspective to organize the contributions of the different force carriers to atomic energy levels. The advantage of this approach is threefold: first, we can disentangle the leading contribution in an efficient and minimal way, thus simplifying computations. Second, we work in a framework in which we have control over the origin and nature of divergences and their associated counterterms. On top of this, we can keep track of the size of the uncomputed terms, thus allowing for a robust error determination.

The potential nonrelativistic EFT that describes the effect of new force carriers in energy shifts is reached by organizing the different scales in the problem. Bound states

are typically nonrelativistic systems in which there are three clearly differentiated energy regimes:

- Hard scale: $m_r = \frac{m_1 m_2}{m_1 + m_2} \sim m_1 \sim m_2$,
- Soft scale: $a_0^{-1} = m_r Z \alpha \sim |\mathbf{p}| \sim 1/r$,
- Ultrasoft scale: $m_r \alpha^2 \sim E$,

where α is the hyperfine structure constant, $m_{1,2}$ are the masses of the bound state components, m_r its reduced mass, E its typical binding energy and $\mathbf{p} = m_r v$ (r) the typical momentum (size). In a bound system, the hard and soft scales can be integrated out. The resulting EFT naturally provides a Schrödinger-like formulation of the bound-state problem while keeping the quantum field theory nature of the interaction with ultrasoft degrees of freedom, and introducing the information of the high-energy modes (also of a quantum field theory nature) in the Wilson coefficients of the theory [19–21]. Given the large amount of precision tests of QED, the contribution of the new force cannot be large compared to the contribution of photons. Therefore, we consider it to be a perturbation to the Coulomb potential, rather than solving the Schrödinger equation exactly. The latter is equivalent to a resummation of higher order effects which will overall amount to a small perturbation of the leading effect, while breaking the power counting of the EFT.

The way in which the new physics effects enter the EFT will depend on the size of m_ϕ . We will distinguish two different EFTs: one where m_ϕ is light, i.e. of the order of the soft scale or smaller, and another where it is heavy, i.e. it scales like the bound state masses (hard scale). We will see that the matching between these two theories is smooth, as it should be. The full EFT for the force carriers in Eq. (2.1) is presented in Appendix A.

The Lamb shift in atoms with components of different mass is given by the energy difference of the $2p$ and $2s$ spin-averaged states $E_{\text{LS}} = E(2p_{1/2}) - E(2s_{1/2})$. This means that only spin-independent interactions like those of vectors and scalars will contribute.¹

The leading order potentials from a new vector [13, 23] or scalar exchange [16], contributing to the LS can be expressed in a compact way as ($X = V, S$)

$$V_{\text{LS}}(r) = \begin{cases} c_X \frac{g_X^{(1)} g_X^{(2)}}{4\pi r} e^{-m_\phi r} & \text{for } m_\phi \lesssim a_0^{-1}, \\ \frac{d_S^{(X)}}{m_1 m_2} \delta^{(3)}(r) & \text{for } m_\phi \sim m_r, \end{cases} \quad (2.2)$$

¹This is not the case for particle-antiparticle states such as positronium, where measurements of non-spin averaged transitions are carried out, and thus get contributions from spin-dependent forces. This was studied in detail in [22].

where $c_V = 1$, and $c_S = -1$. The energy shift produced by this potential can be obtained with the expectation values compiled in Appendix B, which gives

$$E_{\text{LS}} = \begin{cases} -\frac{c_X g_X^{(1)} g_X^{(2)} a_0 m_\phi^2}{8\pi(1 + a_0 m_\phi)^4} & \text{for } m_\phi \lesssim a_0^{-1}, \\ -\frac{c_X g_X^{(1)} g_X^{(2)}}{8\pi a_0^3 m_\phi^2} & \text{for } m_\phi \sim m_r, \end{cases} \quad (2.3)$$

where $a_0 = 1/(m_r Z \alpha)$ is the atomic Bohr radius. In (2.3), the leading correction to both regimes of m_ϕ comes from a tree level exchange, and so the upper relation is equivalent to resumming all the series expansion in $1/m_\phi$ in the heavy mass theory. Note that for $Z > 1$, $g_X^{(N)} = Z g_X^{(p)}$.

We observe that a scalar particle gives an opposite sign contribution with respect to a vector dark force for a fermion-fermion potential. Hence, we could in principle envision a scenario where the LS contributions are canceled among different particles. Note that this is different with respect the $g-2$ case where cancellations are possible without the necessity to add new matter [24]. Furthermore, as we will see in the next section, combining HFS and LS measurements provide a test for dark forces free from possible cancellations. The reason is that a vector force gives a non-zero contribution to the HFS, while scalars do not.

3 Testing dark forces via Hyperfine splitting measurements

We consider the hyperfine splitting of the $1s$ states $E_{\text{HF}} = E(1s^{f=1}) - E(1s^{f=0})$. In this case, only the light axial-vector contributes to this splitting at leading order in the non-relativistic expansion (\mathbf{p}/m_r)

$$V_{\text{HF,A}}(r) = \begin{cases} -\frac{g_A^{(1)} g_A^{(2)}}{\pi r} \mathbf{S}_1 \cdot \mathbf{S}_2 & \text{for } m_\phi \lesssim a_0^{-1}, \\ -\frac{4d_v^{(A)}}{m_1 m_2} \delta^{(3)}(r) \mathbf{S}_1 \cdot \mathbf{S}_2 & \text{for } m_\phi \sim m_r, \end{cases} \quad (3.1)$$

where \mathbf{S}_i refers to the spin of particle- i and $d_v^{(A)}$ can be found in (A.9).

The energy shift produced by this potential is again computed with the results in Appendix B and gives

$$E_{\text{HF,A}} = \begin{cases} -\frac{4g_A^{(1)} g_A^{(2)}}{\pi a_0 (2 + a_0 m_\phi)^2} & \text{for } m_\phi \lesssim m_r \alpha \sim a_0^{-1}, \\ -\frac{4g_A^{(1)} g_A^{(2)}}{\pi a_0^3 m_\phi^2} & \text{for } m_\phi \sim m_r, \end{cases} \quad (3.2)$$

where again, as was the case for the Lamb shift, the heavy- m_ϕ limit of the expression for light mass naturally reproduces the heavy mass one, since both come from tree level exchange.

There is no contribution from a scalar to the hyperfine splitting up to $\mathcal{O}(\mathbf{p}^2/m_r^2)$, while the vector and pseudo-scalar contributions can be compactly expressed by the potential ($X = V, P$)

$$V_{\text{HF}}(r) = \begin{cases} h_X \frac{g_X^{(1)} g_X^{(2)}}{6\pi m_1 m_2} \left(\frac{m_\phi^2 e^{-m_\phi r}}{r} - 4\pi \delta^{(3)}(r) \right) \mathbf{S}_1 \cdot \mathbf{S}_2 & \text{for } m_\phi \lesssim a_0^{-1}, \\ -\frac{4d_v^{(X)}}{m_1 m_2} \delta^{(3)}(r) \mathbf{S}_1 \cdot \mathbf{S}_2 & \text{for } m_\phi \sim m_r, \end{cases} \quad (3.3)$$

with $h_V = 1, h_S = 0, h_P = -\frac{1}{2}$ and where now $d_v^{(V)}$ can be found in (A.7) and $d_v^{(P)}$ in (A.13).

The vector and pseudo-scalar the energy shift is then

$$E_{\text{HF}} = \begin{cases} -h_X \frac{8g_X^{(1)} g_X^{(2)}}{3\pi a_0^3 m_1 m_2} \frac{1 + a_0 m_\phi}{(2 + a_0 m_\phi)^2} & \text{for } m_\phi \lesssim m_r \alpha \sim a_0^{-1}, \\ -\frac{4d_v^{(X)}}{\pi a_0^3 m_1 m_2} & \text{for } m_\phi \sim m_r. \end{cases} \quad (3.4)$$

Now, the energy shift in the light mass EFT comes from a tree-level exchange, while the contribution from the heavy mass EFT arises from the matching onto the one-loop diagrams in the full theory, as graphically described Fig. 1. This produces a non-trivial matching between the heavy and light mass theories

$$\lim_{m_\phi \rightarrow \infty} E_{\text{HF}} \Big|_{\text{light}} = \lim_{m_\phi \rightarrow 0} E_{\text{HF}} \Big|_{\text{heavy}} = -h_X \frac{8g_X^{(1)} g_X^{(2)}}{3\pi a_0^4 m_1 m_2 m_\phi}. \quad (3.5)$$

thus providing a theory for all the possible range of m_ϕ .

The interpretation of this finding is that the leading contribution for a heavy vector/pseudoscalar is not a tree level contribution but rather a contribution at one-loop. This becomes clear if we consider the tree-level potential in momentum space for a heavy pseudoscalar mediator

$$\tilde{V}(\mathbf{q}) = \frac{g_P^{(1)} g_P^{(2)}}{4m_1 m_2 m_\phi^2} (\boldsymbol{\sigma}_1 \mathbf{q})(\boldsymbol{\sigma}_2 \mathbf{q}) \quad (3.6)$$

which produces a position space potential $\sim 1/r^5$ with a divergent expectation value. This hints the presence of a less suppressed contribution with a finite expectation value that can then provide the counterterm to regularize the tree-level divergent contribution. This is a clear example of the power of using EFTs to organize computations. The contribution

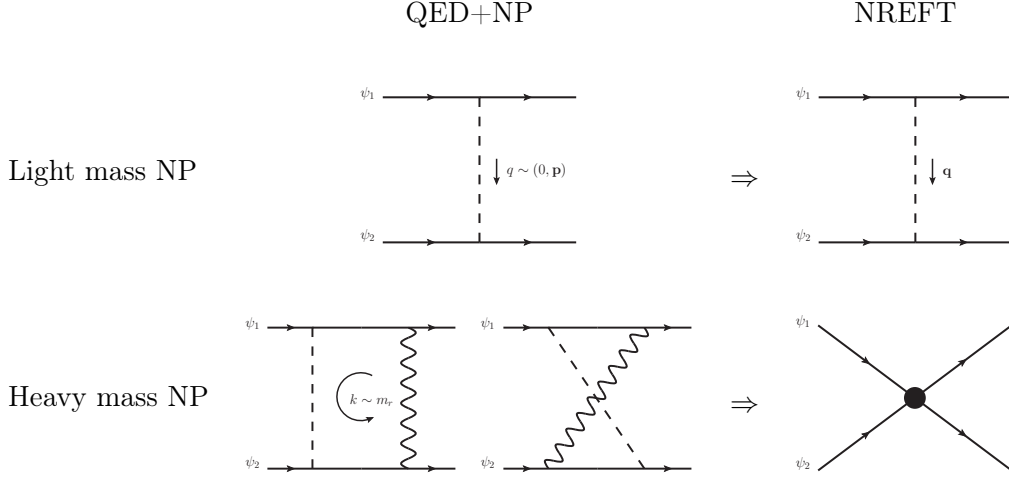


Figure 1. Graphic representation of the matching between the full theory and the NREFT for the HF pseudo-scalar potential in the light and heavy mass theories. Continuous lines represent the fermionic components of the bound state, while dashed and wiggly lines represent the pseudoscalar particle and the photon respectively.

of the heavy mass vector/pseudoscalar mediators to the HFS is a new result. It extends the computation for the vector case in [25], which considers only the extremely heavy case $m_\phi \gg m_1, m_2$.

The results for the ground-state can be easily extended to the $2s$ HF splitting, $E_{\text{HF}2} = E(2s^{f=1}) - E(2s^{f=0})$. The energy shift produced by the HF axial potential in (3.1) is

$$E_{\text{HF}2,A} = \begin{cases} -\frac{g_A^{(1)} g_A^{(2)}}{4\pi} \frac{1 + 2a_0^2 m_\phi^2}{a_0(2 + a_0 m_\phi)^4} & \text{for } m_\phi \lesssim m_r \alpha \sim a_0^{-1}, \\ -\frac{g_A^{(1)} g_A^{(2)}}{2\pi a_0^3 m_\phi^2} & \text{for } m_\phi \sim m_r, \end{cases} \quad (3.7)$$

and for the vector and pseudoscalar in (3.3)

$$E_{\text{HF}2} = \begin{cases} -h_X \frac{g_X^{(1)} g_X^{(2)}}{24\pi a_0^3 m_1 m_2} \frac{a_0 m_\phi (a_0 m_\phi (8a_0 m_\phi + 11) + 8) + 2}{(a_0 m_\phi + 1)^4} & \text{for } m_\phi \lesssim m_r \alpha \sim a_0^{-1}, \\ -\frac{d_v^{(X)}}{2\pi a_0^3 m_1 m_2} & \text{for } m_\phi \sim m_r. \end{cases} \quad (3.8)$$

4 Testing dark forces via $1s - 2s$ splitting measurements

The $1s - 2s$ splitting is typically given by the energy difference $2^{2f+1}s - 1^{2f+1}s$ with $f = 0, 1$, in systems of equal mass components such as positronium or true muonium, or $2s_{1/2}^f - 1s_{1/2}^f$

with $f = 0, 1$, in atoms with different mass components, such as hydrogen-like atoms or muonium. Since this energy difference does not involve spin-averaged states, it gets contributions both from the LS and the HF potentials described in the previous sections.

For the vector, scalar and axial particles, the potential is the leading order Yukawa-like one and we obtain,

$$E_{1S2S} = \begin{cases} f_X^{(s)} \frac{g_X^{(1)} g_X^{(2)}}{16\pi a_0} \left(\frac{2a_0^2 m_\phi^2 + 1}{(a_0 m_\phi + 1)^4} - \frac{16}{(a_0 m_\phi + 2)^2} \right) & \text{for } m_\phi \lesssim m_r \alpha \sim a_0^{-1}, \\ -f_X^{(s)} \frac{7g_X^{(1)} g_X^{(2)}}{8\pi a_0^3 m_\phi^2} & \text{for } m_\phi \sim m_r, \end{cases} \quad (4.1)$$

with $f_V^{(0)} = f_V^{(1)} = 1$, $f_S^{(0)} = f_S^{(1)} = -1$, $f_A^{(0)} = 3$, $f_A^{(1)} = -1$. The case of the pseudoscalar is again more interesting as the potential starts at $\mathcal{O}(1/m_r^2)$

$$E_{1S2S,P} = \begin{cases} \frac{(3-4s)g_P^{(1)} g_P^{(2)}}{192\pi a_0^3 m_1 m_2} \left(14 - \frac{16a_0^2 m_\phi^2}{(a_0 m_\phi + 2)^2} + \frac{a_0^2 m_\phi^2 (2a_0^2 m_\phi^2 + 1)}{(a_0 m_\phi + 1)^4} \right) & \text{for } m_\phi \lesssim m_r \alpha, \\ \frac{-7(3-4s)d_v^{(P)}}{8\pi a_0^3 m_1 m_2} & \text{for } m_\phi \sim m_r. \end{cases} \quad (4.2)$$

There are currently no competitive measurements of the $1s - 2s$ splitting in muonic atoms, although they are expected to be a part of the new era of muonic experiments.

5 Probing dark forces via laser muonic spectroscopy

Muonic atoms are exotic hydrogen-like atoms where an electron is replaced by a muon. The spectroscopy of muonic atoms offers an interesting opportunity to extract properties of the nucleus with high accuracy. The reason is that the muon is lighter than the electron, and hence its wave function has a larger overlap with the nucleus. X-ray spectroscopy of muonic atoms has for a long time been used to determine absolute charge radii for nuclei above carbon [26]. For lighter atoms instead Lamb Shift measurements, due to their weak dependence on the Rydberg constant, provide the possibility of measuring the nucleus radius with better precision with respect to other experimental limits [27], that is elastic electron-nucleus scattering measurements and high-precision laser spectroscopy in standard atoms. This is the strategy followed by the CREMA experiment at the PSI [28, 29]. The first measurement carried out there was on muonic hydrogen in 2010, and led to a new measurement of the proton charge radius one order of magnitude more precise than the previous ones. Nevertheless, this new, more precise method yielded a measurement 4% smaller than the world value. The large discrepancy led the scientific community to revise

the previous determinations (from hydrogen spectroscopy and electron-proton scattering) and, in special, their error determination (see e.g. [27] for a recent review). This has been followed by newer, more precise measurements of hydrogen energy levels, which tend to confirm the smaller proton radius.² Further measurements, also at PSI, of the Lamb shift in muonic deuterium [33] and, more recently, in muonic helium-4 ions ($\mu^4\text{He}$) [34] have followed. Therefore, the present experimental situation of muonic atoms is the perfect testing ground for new muon-related force carriers.

Dark forces might modify atomic energy levels and hence for a given transition $a \rightarrow b$ the agreement between theory and experiment would imply that:

$$|\Delta E_{a \rightarrow b}^{\text{BSM}}| < |\Delta E_{a \rightarrow b}^{\text{exp}} - \Delta E_{a \rightarrow b}^{\text{theo}}| \lesssim 2\sigma_{\text{max}}, \quad (5.1)$$

where $\Delta E_{a \rightarrow b}^{\text{exp}}$ is the experimental measurement and $\Delta E_{a \rightarrow b}^{\text{theo}}$ the theoretical prediction, σ_{max} represents instead the biggest source error, that is:

$$\sigma_{\text{max}} \equiv \text{Max}(\sigma_{\text{exp}}, \sigma_{\text{theo}}). \quad (5.2)$$

Let us now present the values of σ_{max} which we will use in the next subsections to constrain dark forces.

Lamb Shift measurements

System	Lamb shift			
	Exp. (MHz)	Theo. (MHz)	σ_{max} (MHz)	σ_{proj} (MHz)
H	909.8717(32)[18]	909.8742(3)	$3.2 \cdot 10^{-3}$	$0.3 \cdot 10^{-3}$
	Exp. (meV)	Theo. (meV)	σ_{max} (meV)	σ_{proj} (meV)
μH	202.3706(23)[28, 29]	202.397(33)	$33 \cdot 10^{-3}$	$13 \cdot 10^{-3}$
μD	202.8785(34)[33]	202.869(22)	$22 \cdot 10^{-3}$	$7 \cdot 10^{-3}$
$\mu^4\text{He}$	1378.521(48)[34]	1377.54(1.46)	1.46	0.46

Table 1. Table for the theoretical and experimental predictions for the Lamb shift in different muonic systems as well as in hydrogen. See the text for references to the theoretical computations and the origin of the projected uncertainty.

Lamb Shift measurements have been performed on μH , μD and $\mu^4\text{He}$ at PSI³ providing the most accurate value of the nucleus charge radius for these atoms. We report in Table 1

²Note however that, at present, one of the new hydrogen measurements at Paris [30] still gives a larger value for the proton radius. Given that an independent measurement of the same energy shift at MPQ [31], and other independent determinations [18, 32] agree with the smaller proton radius value, we consider this to be a remaining tension for some experiments, which should, nevertheless, be clarified.

³We do not include in our analysis measurements for $\mu^3\text{He}$ as they are so far preliminary [35].

both the experimental and theoretical values for these transitions including also the regular hydrogen (H) latest Lamb Shift measurement. We consider also the projection for realistic improvements on the uncertainty of each system. In the following we provide a brief explanation on how the theoretical predictions are obtained and how the future projections are reached.

- **Hydrogen H** The theoretical prediction is taken from [36] using the value of the proton radius from muonic hydrogen measurements [28, 29]. We compare it to the latest experimental result measured in [18]. In this case, the theoretical prediction is more accurate than the experimental measurement, and so as a future projection we consider that combined experimental measurements can reach a factor 10 improvement and reach the theoretical precision.
- **Muonic Hydrogen μH** For the theoretical prediction we use the computation in [21] with the proton radius obtained from the latest hydrogen spectroscopic measurements in [18, 31, 32] combined (we do not consider the measurement in [30] which predicts a much larger value for the proton radius). We consider that this uncertainty could be improved by a factor $\sim 1/3$ when the proton radius uncertainty reaches the precision of the direct determinations from muonic hydrogen.
- **Muonic Deuterium μD** For the theoretical prediction we use the QED computations compiled in [33] from [37] together with the deuteron radius obtained from hydrogen/deuterium $1s - 2s$ isotope shift measurement [38, 39] corrected by the three photon exchange [40] with the proton radius from the muonic hydrogen Lamb shift measurement [28, 29], and the polarizability correction from chiral EFT computed in [41]. Here, it is the theoretical prediction that limits the accuracy. The theoretical error is fully dominated by the polarizability contribution. Recent studies that combine chiral EFT with a dispersive analysis propose an improvement in the uncertainty of almost a 50% [42] with still room for improvement once future measurements of the deuteron electrodisintegration at the MAMI A1 and MESA experiments are carried out. We therefore consider a projected refinement of the theoretical uncertainty by a factor $\sim 1/3$.
- **Muonic Helium $\mu^4\text{He}$** We consider the latest experimental measurement in [34] and the theoretical analysis in [43]. The bulk of the theoretical uncertainty is given by the poor measurement of the ^4He radius from electron scattering experiments [44]. We consider a reliable improvement of this measurement that would come e.g. from the already ongoing $\mu^3\text{He}$ experiment at PSI in combination with new measurements of

the isotope shift [45, 46]. Assuming the preliminary result for ^3He charge radius [35], we would obtain the ^4He charge radius with an accuracy of ~ 0.001 fm, thus lowering the theoretical uncertainty of the Lamb shift to 0.46 meV. Actually, also the $2p$ fine structure of the $\mu^4\text{He}$ has been measured in [34], but the bounds provided by this transition will be very similar in size to the ones from the Lamb shift presented here.

Hyperfine Splitting measurements

Table 2 presents both the theoretical and experimental predictions of the hyperfine splitting in different muonic systems as well as in hydrogen. We consider also the projection for realistic improvements on the uncertainty of each system. All the hyperfine experimental measurements considered here have the common characteristic that the experimental uncertainty is larger than the theoretical one, thus, as a future projection, we consider that the experimental precision could reach the theoretical one in upcoming experiments. We do not include the muonic deuterium $2s$ hyperfine measurement due to the recently found tension between the experimental and theoretical determinations [47].

- **Hydrogen H** The $1s$ HFS in hydrogen is one of the most accurate measurements ever made (see e.g. [48]). However, the precision of its theoretical description is limited by the presence of nuclear effects. Therefore, the best probe for new physics is actually the measurement of the $2s$ HFS, where we use the very precise $1s$ experimental measurement to quantify the finite size effects in the theoretical prediction. For this we use the theoretical analysis in [49], where analytical computation of the shift $8E(2s) - E(1s)$ (free of finite size effects) is used. The precision here is limited by the latest experimental measurement [50].
- **Muonic Hydrogen μH** For the muonic hydrogen $2s$ HFS we consider the experimental measurement of [28, 29] and compare it to the theoretical prediction presented in [51], where the main nuclear size effect, the two photon exchange contribution, has been computed from the very precise $1s$ measurement in regular hydrogen. Finally, we consider the future proposed experiments that will measure the ground-state HFS in muonic hydrogen [52–54] with an uncertainty that could reach below the μeV . As in the case of regular hydrogen, since the bulk of the HFS theoretical uncertainty still comes from two-photon exchange effects, this new very precise measurement could be used to further reduce the uncertainty of the $2s$ theoretical prediction. By getting rid of the experimental error in the two-photon-exchange [51] we consider a feasible future improvement of the uncertainty of a factor $\sim 1/10$.

System		2s Hyperfine		
	Exp. (MHz)	Theo. (MHz)	σ_{max} (Hz)	σ_{proj} (Hz)
H	177.5568343(67) [50]	177.5568382(3)	6.7	0.3
	Exp. (meV)	Theo. (meV)	σ_{max} (μeV)	σ_{proj} (μeV)
μH	22.8089(51) [28, 29]	22.812(3)	5.1	0.5
System		1s Hyperfine		
μH	–	182.62(2)	–	20

Table 2. Table for the theoretical and experimental predictions of the hyperfine splitting in different muonic systems as well as in hydrogen. See the text for references to the theoretical computations and the origin of the projected uncertainty.

5.1 Spin-independent dark forces

In this section we discuss the sensitivity of the measurements previously discussed to spin-independent dark forces, that is, forces mediated by either a new scalar or a vector. We will present a comparison between this and other model independent laboratory probes. It is important to notice though that both spin independent and spin dependent new forces coupled to muons and protons are strongly constrained by astrophysical bounds such as the supernova SN1987A explosion [55].

Our main findings are captured in Fig. 2 and Fig. 3.

- Fig. 2 presents the sensitivity of the Lamb shift measurements at PSI on μH , μD , and $\mu^4\text{He}$ and for the vector case also of the HFS measurements. In the right panel we assume no coupling to the neutrons, i.e. $g^n = 0$, while on the left panel we consider a scenario with isospin preserving couplings such that $g^n = g^p = g^N$. In both cases, we notice that the μD is the measurement with the strongest sensitivity for masses above 1 MeV, both with respect to the other muonic measurements and to other indirect laboratory probes (grey regions), i.e. probes which do not depend on the production and subsequent decay of the new force mediator. The strongest existing bound on $g^\mu \times g^p$ comes from the measurements on the $3d_{5/2} - 2p_{3/2}$ transitions in muonic 24Mg and 28Si [26] (grey region in the left panel of Fig. 2). If the new particle couples also to neutrons, as it happens naturally in many new physics scenarios i.e. [13, 16], the neutron coupling g^n is constrained by low-energy neutron scattering experiments up to masses ~ 20 MeV. In the region of interest, the strongest bound comes from [56] (see [13] for an overview of these constraints). Hence, in the right panel of Fig. 2 we present the bound from $g_{g2}^\mu \times g_{scattering}^n$ as a darker grey region (g_{g2}^μ is the 10σ constraint on the muon coupling from the $g - 2$ measurement [57] and $g_{scattering}^n$ [56]).

Even though the μ D bound is only slightly stronger than the existing one, it is more solid than the neutron scattering due to several uncertainties in the latter one (see [13] for a brief discussion). Finally, we notice that the bounds from HFS measurements (three green lines), valid only in the case of a vector mediator, are far less strong than the ones obtained by these old measurements. This is also true considering the projection for future improvements. This is easily explained by the suppression of the HFS contribution from a vectorial new force compared to the Lamb shift.

- In Fig. 3 we compare the bounds from muonic atoms to the bounds coming from other systems. The left panel presents the comparison of the reach of the μ D measurement to the one of standard atoms considering both the hydrogen LS measurement (Table 1) and isotope shift (IS) measurements⁴. Since all these measurements are sensitive to different couplings (electrons, protons, neutrons or protons) we assume $g^p = g^n = g^N$ and $g^e = g^\mu$. In Fig. 3 we present for the first time an updated bound from the LS measurement on standard hydrogen considering the latest measurement [18] and the updated measurement of the proton charge radius from muonic hydrogen. We find that this is, at the moment, the strongest bound from atomic physics spectroscopy in the light mass regime. In the near future this could be overcome by the IS measurements on helium [6]. An even stronger sensitivity could be reached by reaching Yb measurements [11, 12], see [12] for a discussion on the treatment of non linearity. We see that the μ D bound is the strongest among the existing ones for $m_\phi > 1$ MeV overcoming for $m_\phi > 10$ MeV also the projections [6, 12]. The right panel presents the comparison between atomic probes including also the $2s$ HFS sensitivity for regular hydrogen. This bound is valid only for the vector case. We see that a future improvement of the experimental accuracy to match the theoretical one, could provide the best sensitivity among atomic probes for masses above 100 MeV.

⁴In this case two approaches are viable, either the one of bounding new physics via σ_{max} [6] also followed in this work or via the Kings plot measurements [11].

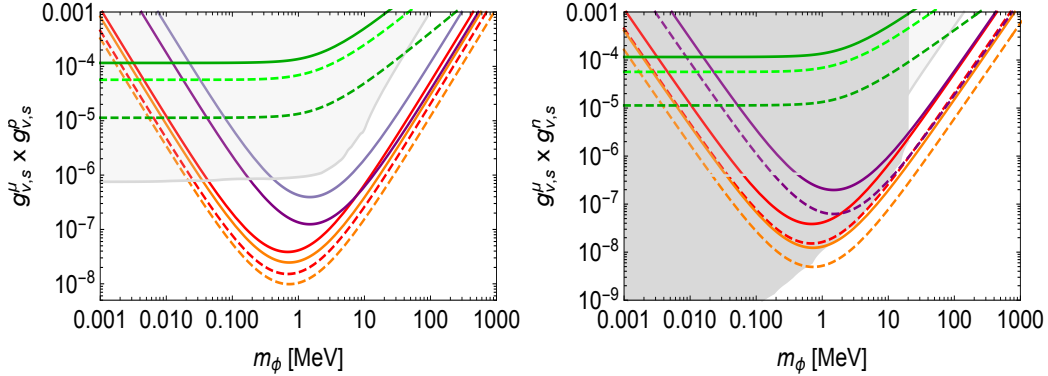


Figure 2. *Left plot:* constraints on the dimensionless coupling $g^\mu \times g^p$ as a function of the scalar/vector mass m_ϕ . All the lines correspond to the bounds coming from muonic atoms spectroscopy, see Table 1 and Table 2 for the experimental and theoretical precision. Dashed lines represent the future projections obtained in Tables 1 and 2. The red/orange/purple curves represent the bound coming from $\mu H/\mu D/\mu^4\text{He}$ Lamb shift measurements respectively. The green curves correspond to the bound coming from HFS measurements and apply only in the case of a vector mediator. The two darker green are the constraints from the $2s$ HFS, while the lighter green is the projection for the $1s$ HFS considering the projection for the FAMU experiment, see Table 2. The light grey region corresponds to the region excluded by the X-ray measurements on the $3d_{5/2} - 2p_{3/2}$ transitions in muonic ^{24}Mg and ^{28}Si [26]. *Right plot:* the lines correspond to the same transitions as in the left panel with the difference that we consider here a scenario where the new force couples both with proton and neutrons assuming $g^p = g^n = g^N$. Hence, the constraint is on $g^\mu \times g^n$ where g^n indicates the nucleon coupling. The dark grey region corresponds to $g_{g2}^\mu \times g_{scattering}^n$, where g_{g2}^μ is the bound from the muon $g-2$ at 10σ [57]. The neutron coupling g^n is constrained by low-energy neutron scattering experiments up to masses ~ 20 MeV, in the region of interest the strongest bound comes from [56] (see [13] for an overview of these constraints).

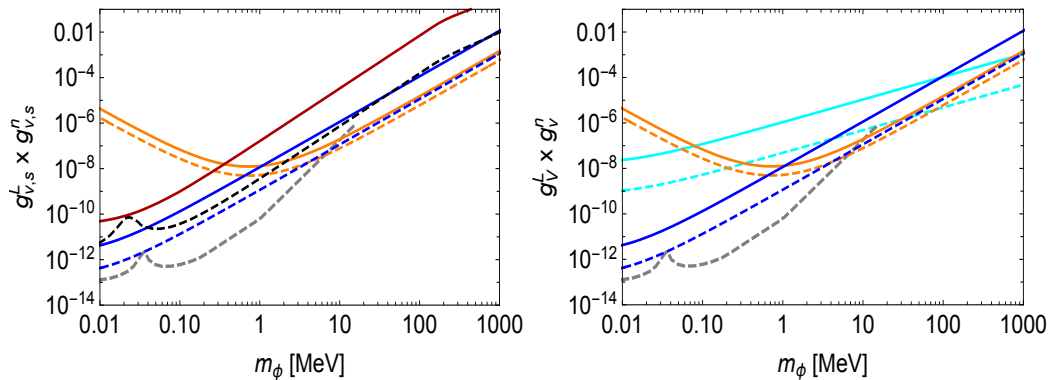


Figure 3. *Left plot:* comparison between the sensitivity reached by electronic and muonic atomic spectroscopy considering a new dark force mediated by either a scalar or a vector new particle. We assume $g^e = g^\mu$ and $g^p = g^n = g^N$. The orange line represents the bound from μ D spectroscopy. The blue curve represents the updated bound from the latest H Lamb Shift measurement [18] (considering also the muonic hydrogen measurement for the proton charge radius). Dashed lines correspond to future improvements. The grey dashed line represents the projection for the Yb IS measurement as proposed in [12], while the dashed black is the projection for the IS He⁴ bound as explained in [6]. *Right plot:* this plot applies only to the case where the new force is mediated by a vector new particle, since we also include (cyan lines) the bounds coming from 2s HFS in regular hydrogen (see Table 2).

5.2 Spin-dependent dark forces

We first study the sensitivity to a new axial dark force. Such a scenario has been mainly studied in the context of experimental anomalies such as the Beryllium anomaly (see for instance [58]). Fig. 4 presents the sensitivity of HFS in muonic spectroscopy considering the present bound from the CREMA $2s$ HFS measurement in muonic hydrogen and the projections also for the future FAMU measurement of the $1s$ HFS. In the right panel, the sensitivity of muonic spectroscopy is compared to the one of muonium HFS [59] and, for the first time, to the hydrogen $2s$ HFS, assuming equal couplings to all fermions. We notice that the future hydrogen $2s$ HFS measurement will provide the strongest probe of such dark force among precision atomic spectroscopy. We checked that the $2s$ HFS measurement provides a stronger bound than the $1s$ HFS presented in [5]: indeed, the sensitivity of the latter is limited by the theoretical uncertainty.

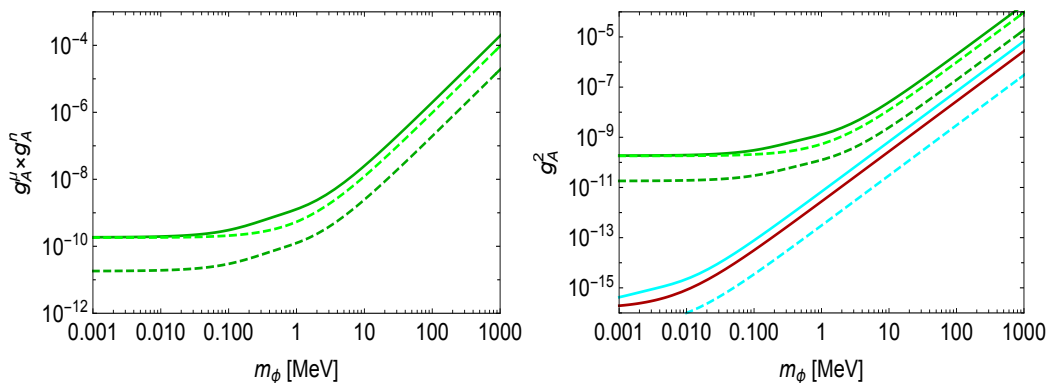


Figure 4. *Left plot:* Sensitivity to a new dark axial force coupled to protons and muons of the HFS measurement on μH . Dark green lines correspond to the $2s$ HFS and light green dashed the projection for the $1s$ HFS measurement proposed by the FAMU experiment, see Table 2 for details and references. Dashed lines correspond to projected future improvements. *Right plot:* Comparison between the muonic measurements and other HFS measurements on hydrogen and muonium μe assuming that $g_\mu^A = g_p^A = g_e^A$.

Finally, we consider the case of a dark force mediated by a light pseudo-scalar, which are ubiquitous in many BSM scenarios (for a review [60, 61]). In the left panel of Fig. 5, we can appreciate how the overall sensitivity of spectroscopy is very limited compared to other force carriers, the reason being the mass suppression of its leading potential. The right panel of Fig. 5 presents the comparison with the bound from the $2s$ HFS in regular hydrogen, considering a scenario where $g^e = g^\mu \frac{m_e}{m_\mu}$. In this case, the muonic spectroscopy provides the strongest bound (also taking into account future projections) for sufficiently heavy particles ($m_\phi \gtrsim 1$ MeV).

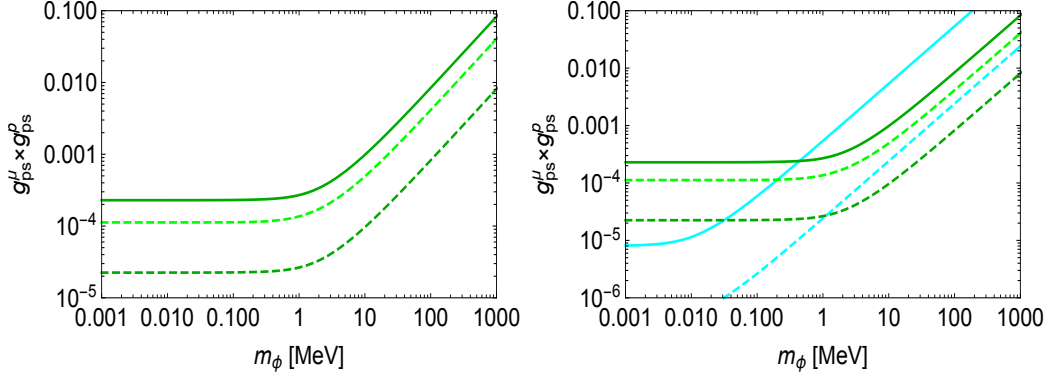


Figure 5. *Left Plot:* Sensitivity to a light axion-like particle coupled to muons and protons of the μH HFS measurements and projections. The dark green curves correspond to the $2s$ HFS present (solid) and future (dashed) bounds, while the light dashed green to the future $1s$ HFS FAMU measurement, see Table 2. *Right plot:* we consider a scenario where $g^e = g^\mu \frac{m_e}{m_\mu}$ and compare μ HFS measurements to the $2s$ HFS on regular hydrogen.

6 Conclusions

Precision atomic spectroscopy offers a powerful and robust probe of the existence of new light dark sectors. In this paper we studied the sensitivity of the Lamb Shift and Hyperfine splitting measurements in muonic atoms at PSI to spin-independent and spin-dependent dark forces. Among the atomic systems, muonic atoms are particularly sensitive to a new intermediate (MeV-GeV) scale. This is a rather unique feature in the MeV-GeV region (other examples include the leptonic gyromagnetic factor [62, 63] or electric dipole moments [64]) since most of the other probes both at the precision (such as rare meson decays) and intensity frontier depend on the decay modes of the new particle.

Our main findings are the following:

- We develop the EFT that describes the leading effect of a new (pseudo-)vector or (pseudo-)scalar boson of *any mass* at atomic energies. While this was already studied for light masses (of the order of the inverse size of the atom) the computation for intermediate and large masses of the one-loop matching coefficients is new. In our work this is particularly relevant for the description of the vector and pseudo-scalar bosons hyperfine splitting, where the leading effect is a one-loop effect rather than a tree level exchange. The EFT presented in Appendix A however, is general and can be used to describe any effect at atomic energies.
- We find that the Lamb Shift CREMA measurement on μD provides the strongest indirect laboratory bounds on the spin-independent bound $g^\mu \times g^n$ couplings for $m_\phi >$

1 MeV region. Moreover, we find that for $m_\phi > 1$ MeV (where ϕ is the new particle mediating such a force) the present CREMA measurements supersede all existing atomic measurements including isotope shift measurements. Furthermore, for $m_\phi > 10$ MeV this is true also taking into account future projections [6, 11].

- We discussed for the first time the full expression and the importance of taking into account the contribution of a vector new force to the HFS: we show that the future HFS $2s$ measurement in Hydrogen would provide the strongest bound for masses $m_\phi > 100$ MeV, see Fig. 3 .

Acknowledgments

The work of CP is supported by the DFG within the Emmy Noether Programme under grant DY130/1-1 and by the NSFC and the DFG through the funds provided to the Sino-German Collaborative Research Center TRR110 ‘‘Symmetries and the Emergence of Structure in QCD’’ (NSFC Grant No. 12070131001, DFG Project-ID 196253076 - TRR 110).

A The EFT for new particle interactions

We start by considering an additional (flavor preserving) interaction with the SM fermions that can be vector (V), scalar (S), pseudo-scalar (P) or axial-like (A) as in Eq. (2.1).

A.1 The nonrelativistic EFT

Since the fermions in a bound state move at very small relative velocity $v \ll 1$, these interactions can be matched onto a nonrelativistic effective field theory (NREFT). For QED this theory is NRQED [65]. The precise shape of this theory will be different depending on the mass of the new particle m_ϕ . We consider a light mass theory where $m_\phi \lesssim m_r \alpha$ and a heavy mass one where $m_\phi \sim m_r$. At order g/m_r^2 , the fermion bilinear interactions are independent of the mediator mass

$$\mathcal{L}_V^{\text{NR}} = \psi^\dagger \left\{ g_V V^0 + \frac{id_k g_V}{2m} (\nabla \mathbf{V} + \mathbf{V} \nabla) - \frac{d_1 g_V}{2m} \boldsymbol{\sigma} \mathbf{B} - \frac{d_2 g_V}{8m^2} [\nabla, \mathbf{E}] - \frac{d_3 g_V}{8m^2} i \sigma^{ij} \{ \nabla^i, E^j \} \right\} \psi - (\psi \rightarrow \chi^c) \quad (\text{A.1})$$

$$\mathcal{L}_A^{\text{NR}} = -g_A \boldsymbol{\sigma} \mathbf{A} - \frac{g_A}{2m^2} d_8 \{ \nabla, \{ \nabla, \boldsymbol{\sigma} \cdot \mathbf{A} \} \} + \frac{g_A}{4m^2} d_9 \{ \boldsymbol{\sigma} \nabla, \nabla \mathbf{A} \} - \frac{g_A}{4m^2} d_{10} [\nabla, (\boldsymbol{\sigma} \nabla) \mathbf{A}] + \frac{g_A}{4m^2} d_{11} i (\nabla \times \mathbf{A}) \nabla - \frac{g_A}{2m} d_{12} \{ \boldsymbol{\sigma} \nabla, A^0 \} - \frac{g_A}{8m^2} d_{12} [\boldsymbol{\sigma} \nabla, (\partial^0 A^0)] - (\psi \rightarrow \chi^c) \quad (\text{A.2})$$

$$\mathcal{L}_S^{\text{NR}} = \psi^\dagger \left\{ g_S A^0 + \frac{d_4 g_S}{8m^2} \{ \nabla, \nabla S + S \nabla \} - \frac{id_5 g_S}{8m^2} \sigma^{ij} \{ \nabla^i, (\nabla^j S) \} \right\} \psi + (\psi \rightarrow \chi^c) \quad (\text{A.3})$$

$$\mathcal{L}_P^{\text{NR}} = \psi^\dagger \left\{ -\frac{d_6 g_P}{2m} \boldsymbol{\sigma} [\nabla, P] + \frac{id_7 g_P}{8m^2} \boldsymbol{\sigma} \{ \nabla, (\partial^0 P) \} \right\} \psi + (\psi \rightarrow \chi^c) \quad (\text{A.4})$$

where ψ (χ^c) is a two-component (anti-)quark field with mass m , $\mathbf{E} = -\nabla V^0 - \partial^0 \mathbf{V}$, $\mathbf{B} = \nabla \times \mathbf{V}$ and $\sigma^{ij} = -i/2[\sigma^i, \sigma^j]$. At leading order we find $d_i = 1$. The vector-like Lagrangian reproduces the well known result for NRQED/QCD [65–67].

We also need to consider the four-fermion interactions

$$\mathcal{L}_X^{\text{NR}} = -\frac{d_s^{(X)}}{m_1 m_2} \psi_1^\dagger \psi_1 \chi_2^{c\dagger} \chi_2^c + \frac{d_v^{(X)}}{m_1 m_2} \psi_1^\dagger \boldsymbol{\sigma} \psi_1 \chi_2^{c\dagger} \boldsymbol{\sigma} \chi_2^c, \quad (\text{A.5})$$

with $X = V, A, S, P$. The Wilson coefficients in (A.5) do depend on the size of the mass of the new particle.

For a light mediator mass, the coefficients start at one loop for different fermion masses⁵ and will not produce the leading effect in any of the energy shifts we consider, thus they are beyond the scope of this work.

For heavy mediator masses $m_\phi \sim m_r$, the new particle is integrated out from the NREFT and its effects can only be seen through contact interactions as in (A.5). We find that for the vector and scalar cases d_s starts at tree level and d_v at one loop while for the pseudo-scalar case both d_v and d_s start at one loop. We have computed the matching of these coefficients at one-loop with the help of the `FeynOnium` code [68]. In the case of different mass components of the bound state, as was noted in [69], only the box-like diagrams contribute. We find:

$$d_s^{(V)} = g_V^{(1)} g_V^{(2)} \frac{m_1 m_2}{2m_\phi^2} + \frac{g_V^{(1)} g_V^{(2)} Z \alpha m_2^2}{4(m_1^2 - m_2^2)\pi} \left[1 + 2(1 - 2x^2) \ln(2x) + \frac{2}{x^3} (1 + 2x^4) \sqrt{x^2 - 1} \ln(x + \sqrt{x^2 - 1}) \right] + (m_1 \leftrightarrow m_2), \quad (\text{A.6})$$

$$d_v^{(V)} = -\frac{g_V^{(1)} g_V^{(2)} Z \alpha m_1 m_2}{4(m_1^2 - m_2^2)\pi} \left[\ln \frac{m_1}{m_2} - \frac{4x^2}{3} \ln(2x) + \frac{4}{3x} (2 + x^2) \sqrt{x^2 - 1} \ln(x + \sqrt{x^2 - 1}) \right] + (m_1 \leftrightarrow m_2), \quad (\text{A.7})$$

$$d_s^{(A)} = g_A^{(1)} g_A^{(2)} \frac{m_1 m_2}{2m_\phi^2} + \frac{g_A^{(1)} g_A^{(2)} Z \alpha m_2^2}{6(m_1^2 - m_2^2)\pi} \left[1 - 2 \ln \frac{m_1}{m_2} - 2 \left(\frac{m_1^2}{m_2^2} + 2x^2 \right) \ln(2x) - \frac{4}{x^3} (1 - x^4) \sqrt{x^2 - 1} \ln(x + \sqrt{x^2 - 1}) \right] + (m_1 \leftrightarrow m_2), \quad (\text{A.8})$$

$$d_v^{(A)} = -\frac{2g_A^{(1)} g_A^{(2)} Z \alpha m_1 m_2}{(m_1^2 - m_2^2)\pi} \left[-\frac{3}{4} \ln \frac{m_1}{m_2} - x^2 \ln(2x) - \frac{1}{x} (1 - x^2) \sqrt{x^2 - 1} \ln(x + \sqrt{x^2 - 1}) \right] + (m_1 \leftrightarrow m_2), \quad (\text{A.9})$$

⁵For fermion-antifermion systems of equal mass, the annihilation diagrams will produce non-zero four-fermion Wilson coefficients already at tree level.

$$d_s^{(S)} = -g_S^{(1)} g_S^{(2)} \frac{m_1 m_2}{2m_\phi^2} - \frac{g_S^{(1)} g_S^{(2)} Z \alpha m_2^2}{(m_1^2 - m_2^2) \pi} \left[\ln(2x) + \frac{1}{x^3} (1-x^2) \sqrt{x^2-1} \ln(x + \sqrt{x^2-1}) \right] \\ + (m_1 \leftrightarrow m_2), \quad (\text{A.10})$$

$$d_v^{(S)} = \frac{g_S^{(1)} g_S^{(2)} Z \alpha m_1 m_2}{2(m_1^2 - m_2^2) \pi} \left[\ln \frac{m_1}{m_2} + \frac{4x^2}{3} \ln(2x) + \frac{4}{3x} (1-x^2) \sqrt{x^2-1} \ln(x + \sqrt{x^2-1}) \right] \\ + (m_1 \leftrightarrow m_2), \quad (\text{A.11})$$

$$d_s^{(P)} = 0, \quad (\text{A.12})$$

$$d_v^{(P)} = \frac{g_P^{(1)} g_P^{(2)} Z \alpha m_1 m_2}{3(m_1^2 - m_2^2) \pi} \left[2x^2 \ln(2x) - \frac{1}{x} (1+2x^2) \sqrt{x^2-1} \ln(x + \sqrt{x^2-1}) \right] \\ + (m_1 \leftrightarrow m_2), \quad (\text{A.13})$$

where $x \equiv m_\phi/(2m_1)$. We have checked that in the massless mediator limit, we recover the results obtained in [69] for NRQED.

A.2 The potential NREFT

Now, in order to obtain a sound EFT with well-defined power counting rules, we can obtain a potential EFT by integrating out the soft scale $m_r \alpha$, where only ultrasoft modes are dynamical [19, 70].

We compile here the full expressions for the position space potentials at order g_X^2/m_r^2 for a vector, axial-vector, scalar and pseudo-scalar mediator between a fermion of mass m_1 and an antifermion of mass m_2 . It is known that there is a certain freedom on the choice of matching scheme from the NREFT to the potential-NREFT [71]. We choose to do the matching off-shell, where potential loops cancel exactly and do not have to be considered. We find for the potentials $V_{XY}(r)$ with $X, Y = V, A, S, P$:

$$V_{VV}(r) = \frac{g_V^{(1)} g_V^{(2)}}{4\pi r} e^{-m_\phi r} + \frac{g_V^{(1)} g_V^{(2)}}{8\pi m_1 m_2} \left[\frac{2\mathbf{S}^2}{3} m_\phi^2 \left(\frac{e^{-m_\phi r}}{r} - 4\pi \delta^{(3)}(r) \right) + \frac{m_\phi}{2} \{ \mathbf{P}^2, e^{-m_\phi r} \} \right. \\ + \left\{ \mathbf{P}^2, \frac{e^{-m_\phi r}}{2r} \right\} + \frac{m_\phi^3}{4} e^{-m_\phi r} - \left(1 - \frac{m_1 m_2}{4m_r^2} \right) \frac{m_\phi^2 e^{-m_\phi r}}{r} + \left(1 - \frac{m_1 m_2}{2m_r^2} \right) 2\pi \delta^{(3)}(r) \\ - \frac{\hat{S}_{12}(\hat{\mathbf{r}})}{2} e^{-m_\phi r} \left(\frac{m_\phi^2}{3r} + \frac{m_\phi}{r^2} + \frac{1}{r^3} \right) - e^{-m_\phi r} (m_\phi r + 1) \frac{\mathbf{L}^2}{r^3} \\ - \left(\frac{m_1 m_2}{2m_r^2} + 1 \right) e^{-m_\phi r} (m_\phi r + 1) \frac{\mathbf{LS}}{r^3} + \frac{m_1^2 - m_2^2}{2m_1 m_2} e^{-m_\phi r} (m_\phi r + 1) \frac{\mathbf{LS}^-}{r^3} \left. \right] \\ + \frac{d_s^{(V)} + 3d_v^{(V)}}{m_1 m_2} \delta^{(3)}(r) - \frac{2d_v^{(V)}}{m_1 m_2} \mathbf{S}^2 \delta^{(3)}(r), \quad (\text{A.14})$$

$$\begin{aligned}
V_{AA}(r) = & 3 \frac{g_A^{(1)} g_A^{(2)}}{4\pi r} e^{-m_\phi r} + \frac{g_A^{(1)} g_A^{(2)}}{2\pi r} e^{-m_\phi r} \mathbf{S}^2 \\
& - \frac{g_A^{(1)} g_A^{(2)}}{16\pi m_1 m_2} \left\{ (2\mathbf{S}^2 - 3) \left[\frac{2(m_1^2 + m_2^2)}{m_1 m_2} \left\{ \mathbf{p}^2, \frac{e^{-m_\phi r}}{2r} \right\} \right. \right. \\
& - m_\phi \text{acon}(\mathbf{p}^2, e^{-m_\phi r}) + 2e^{-m_\phi r} (m_\phi r + 1) \frac{\mathbf{L}^2}{r^3} - \left(\frac{2}{3} - \frac{m_1 m_2}{2m_r^2} \right) \frac{m_\phi^2 e^{-m_\phi r}}{r} \\
& - \frac{1}{2} m_\phi^3 e^{-m_\phi r} + \left. \left(\frac{5}{3} - \frac{m_1 m_2}{2m_r^2} \right) 4\pi \delta^{(3)}(r) \right] + \frac{m_1^2 - m_2^2}{m_1 m_2} e^{-m_\phi r} (m_\phi r + 1) \frac{\mathbf{L}\mathbf{S}}{r^3} \\
& + \frac{m_1^2 + m_2^2}{m_1 m_2} e^{-m_\phi r} (m_\phi r + 1) \frac{\mathbf{L}\mathbf{S}^-}{r^3} - \frac{8m_1 m_2}{m_r^2} \left(\mathbf{S}_1 \cdot \mathbf{p} \frac{e^{-m_\phi r}}{r} \mathbf{S}_2 \cdot \mathbf{p} \right) \\
& + \hat{S}_{12}(\hat{\mathbf{r}}) e^{-m_\phi r} \left(\frac{m_\phi^2}{3r} + \frac{m_\phi}{r^2} + \frac{1}{r^3} \right) \left. \right] + \frac{d_s^{(A)} + 3d_v^{(A)}}{m_1 m_2} \delta^{(3)}(r) - \frac{2d_v^{(A)}}{m_1 m_2} \mathbf{S}^2 \delta^{(3)}(r),
\end{aligned} \tag{A.15}$$

$$\begin{aligned}
V_{SS}(r) = & - \frac{g_S^{(1)} g_S^{(2)}}{4\pi r} e^{-m_\phi r} - \frac{g_S^{(1)} g_S^{(2)}}{8\pi m_1 m_2} \left[- \left(1 - \frac{m_1 m_2}{2m_r^2} \right) \left\{ \mathbf{p}^2, \frac{e^{-m_\phi r}}{r} \right\} - \frac{m_\phi}{2} \left\{ \mathbf{p}^2, e^{-m_\phi r} \right\} \right. \\
& + e^{-m_\phi r} (m_\phi r + 1) \frac{\mathbf{L}^2}{r^3} + \left. \left(1 - \frac{m_1 m_2}{2m_r^2} \right) e^{-m_\phi r} (m_\phi r + 1) \frac{\mathbf{L}\mathbf{S}}{r^3} \right. \\
& + \frac{m_1^2 - m_2^2}{m_1 m_2} e^{-m_\phi r} (m_\phi r + 1) \frac{\mathbf{L}\mathbf{S}^-}{r^3} - \left. \left(1 - \frac{m_1 m_2}{2m_r^2} \right) \frac{m_\phi^2 e^{-m_\phi r}}{2r} \right. \\
& \left. + 4\pi \delta^{(3)}(r) \left(1 - \frac{m_1 m_2}{4m_r^2} \right) - \frac{1}{4} m_\phi^3 e^{-m_\phi r} \right] + \frac{d_s^{(S)} + 3d_v^{(S)}}{m_1 m_2} \delta^{(3)}(r) - \frac{2d_v^{(S)}}{m_1 m_2} \mathbf{S}^2 \delta^{(3)}(r),
\end{aligned} \tag{A.16}$$

$$\begin{aligned}
V_{PP}(r) = & \frac{g_P^{(1)} g_P^{(2)}}{16\pi m_1 m_2} \left[\frac{m_\phi^2 e^{-m_\phi r}}{r} - 4\pi \delta^{(3)}(r) \right] \left(1 - \frac{2}{3} \mathbf{S}^2 \right) \\
& - \frac{g_P^{(1)} g_P^{(2)}}{16\pi m_1 m_2} \hat{S}_{12}(\hat{\mathbf{r}}) e^{-m_\phi r} \left(\frac{m_\phi^2}{3r} + \frac{m_\phi}{r^2} + \frac{1}{r^3} \right) + \frac{d_s^{(P)} + 3d_v^{(P)}}{m_1 m_2} \delta^{(3)}(r) \\
& - \frac{2d_v^{(P)}}{m_1 m_2} \mathbf{S}^2 \delta^{(3)}(r),
\end{aligned} \tag{A.17}$$

where $\hat{S}_{ij}(\hat{\mathbf{r}}) = -4(\mathbf{S}_i \cdot \mathbf{S}_j) + 12(\mathbf{S}_i \cdot \hat{\mathbf{r}})(\mathbf{S}_j \cdot \hat{\mathbf{r}})$. We remark that these are the full potentials up to order g_X^2/m^2 . They complete the results obtained in [72] where all the potentials proportional to $1/m_1^2$ and $1/m_2^2$ and \mathbf{L}^2 (or the equivalent potential loops in the on-shell matching scheme) are missing. The vector potential in the massless mediator limit $m_\phi \rightarrow 0$ reproduces the well-known pNRQED result [19, 21].

For a heavy mass mediator the potentials can be fully expressed in terms of the Wilson

coefficients in Eqs. (A.7)-(A.13) and read

$$V_{XX}(r) = \frac{d_s^{(X)} + 3d_v^{(X)}}{m_1 m_2} \delta^{(3)}(r) - \frac{2d_v^{(X)}}{m_1 m_2} \mathbf{S}^2 \delta^{(3)}(r). \quad (\text{A.18})$$

This completes the pNREFT that describes the effect of a new dark force at atomic energies.

B Expectation values

In order to compute energy shifts from the potentials in appendix A.2 we need to compute the expectation values of the different operators. We give here some general expressions for their computation.

Spin-like expectation values [73]:

$$\begin{aligned} \langle \mathbf{S}^2 \rangle &= s(s+1), & \langle \mathbf{L}\mathbf{S} \rangle &= \frac{1}{2}(j(j+1) - l(l+1) - s(s+1)), \\ \langle \mathbf{L}\mathbf{S}_i \rangle &= \frac{1}{2}(j(j+1) - l(l+1) - s_i(s_i+1)), & \langle \mathbf{L}\mathbf{S}^- \rangle &= 2\langle \mathbf{L}\mathbf{S}_1 \rangle - \langle \mathbf{L}\mathbf{S} \rangle, \\ \langle \hat{S}_{ij}(\hat{\mathbf{r}}) \rangle &= 4 \frac{2l(l+1)s(s+1) - 3\langle \mathbf{L}\mathbf{S} \rangle - 6\langle \mathbf{L}\mathbf{S} \rangle^2}{(2l-1)(2l+3)}. \end{aligned} \quad (\text{B.1})$$

We also compile here a general expression for the relevant radial expectation values:

$$\begin{aligned} \left\langle \frac{e^{-m_\phi r}}{r^x} \right\rangle &= \frac{4(n-l-1)! \left(\frac{a_0 n}{2}\right)^{3-x}}{(a_0^3 n^4) (l+n)!} \sum_{k=0}^{\infty} \frac{\left(-\frac{m_\phi a_0 n}{2}\right)^k \Gamma(k+2l-x+3) \Gamma(-k-l+n+x-2)^2}{\Gamma(k+1) \Gamma(-k+x-1)^2 \Gamma(n-l)^2} \\ &\quad \times {}_3F_2(l-n+1, l-n+1, k+2l-x+3; k+l-n-x+3, k+l-n-x+3; 1), \\ \langle \mathbf{p}^2, \frac{e^{-m_\phi r}}{r^x} \rangle &= \frac{4}{a_0} \left\langle \frac{e^{-m_\phi r}}{r^{x+1}} \right\rangle - \frac{2}{n^2 a_0^2} \left\langle \frac{e^{-m_\phi r}}{r^x} \right\rangle. \end{aligned} \quad (\text{B.2})$$

References

- [1] M.S. Safronova, D. Budker, D. DeMille, D.F.J. Kimball, A. Derevianko and C.W. Clark, *Search for New Physics with Atoms and Molecules*, *Rev. Mod. Phys.* **90** (2018) 025008 [[1710.01833](#)].
- [2] A. Derevianko and M. Pospelov, *Hunting for topological dark matter with atomic clocks*, *Nature Phys.* **10** (2014) 933.
- [3] J. Jaeckel and S. Roy, *Spectroscopy as a test of Coulomb's law: A Probe of the hidden sector*, *Phys. Rev.* **D82** (2010) 125020 [[1008.3536](#)].
- [4] S.G. Karshenboim and V.V. Flambaum, *Constraint on axion-like particles from atomic physics*, *Phys. Rev. A* **84** (2011) 064502 [[1110.6259](#)].
- [5] S.G. Karshenboim, *Precision physics of simple atoms and constraints on a light boson with ultraweak coupling*, *Phys. Rev. Lett.* **104** (2010) 220406 [[1005.4859](#)].
- [6] C. Delaunay, C. Frugiuele, E. Fuchs and Y. Soreq, *Probing new spin-independent interactions through precision spectroscopy in atoms with few electrons*, *Phys. Rev. D* **96** (2017) 115002 [[1709.02817](#)].

- [7] C. Frugiuele, J. Pérez-Ríos and C. Peset, *Current and future perspectives of positronium and muonium spectroscopy as dark sectors probe*, *Phys. Rev. D* **100** (2019) 015010 [[1902.08585](#)].
- [8] D. Antypas, O. Tretiak, K. Zhang, A. Garcon, G. Perez, M.G. Kozlov et al., *Probing fast oscillating scalar dark matter with atoms and molecules*, *Quantum Sci. Technol.* **6** (2021) 034001 [[2012.01519](#)].
- [9] D. Antypas, O. Tretiak, A. Garcon, R. Ozeri, G. Perez and D. Budker, *Scalar dark matter in the radio-frequency band: atomic-spectroscopy search results*, *Phys. Rev. Lett.* **123** (2019) 141102 [[1905.02968](#)].
- [10] M.P.A. Jones, R.M. Potvliege and M. Spannowsky, *Probing new physics using Rydberg states of atomic hydrogen*, *Phys. Rev. Res.* **2** (2020) 013244 [[1909.09194](#)].
- [11] J.C. Berengut et al., *Probing New Long-Range Interactions by Isotope Shift Spectroscopy*, *Phys. Rev. Lett.* **120** (2018) 091801 [[1704.05068](#)].
- [12] J.C. Berengut, C. Delaunay, A. Geddes and Y. Soreq, *Generalized King linearity and new physics searches with isotope shifts*, *Phys. Rev. Res.* **2** (2020) 043444 [[2005.06144](#)].
- [13] C. Frugiuele, E. Fuchs, G. Perez and M. Schlaffer, *Constraining New Physics Models with Isotope Shift Spectroscopy*, *Phys. Rev.* **D96** (2017) 015011 [[1602.04822](#)].
- [14] G.F. Giudice, *The Dawn of the Post-Naturalness Era*, in *From My Vast Repertoire ...: Guido Altarelli's Legacy*, A. Levy, S. Forte and G. Ridolfi, eds. (2019), DOI [[1710.07663](#)].
- [15] M. Battaglieri et al., *US Cosmic Visions: New Ideas in Dark Matter 2017: Community Report*, in *U.S. Cosmic Visions: New Ideas in Dark Matter*, 7, 2017 [[1707.04591](#)].
- [16] P.W. Graham, D.E. Kaplan and S. Rajendran, *Cosmological Relaxation of the Electroweak Scale*, *Phys. Rev. Lett.* **115** (2015) 221801 [[1504.07551](#)].
- [17] J. Beacham et al., *Physics Beyond Colliders at CERN: Beyond the Standard Model Working Group Report*, *J. Phys. G* **47** (2020) 010501 [[1901.09966](#)].
- [18] N. Bezginov, T. Valdez, M. Horbatsch, A. Marsman, A.C. Vutha and E.A. Hessels, *A measurement of the atomic hydrogen Lamb shift and the proton charge radius*, *Science* **365** (2019) 1007.
- [19] A. Pineda and J. Soto, *Effective field theory for ultrasoft momenta in NRQCD and NRQED*, *Nucl. Phys. B Proc. Suppl.* **64** (1998) 428 [[hep-ph/9707481](#)].
- [20] A. Pineda and J. Soto, *Potential NRQED: The Positronium case*, *Phys. Rev. D* **59** (1999) 016005 [[hep-ph/9805424](#)].
- [21] C. Peset and A. Pineda, *The Lamb shift in muonic hydrogen and the proton radius from effective field theories*, *Eur. Phys. J. A* **51** (2015) 156 [[1508.01948](#)].
- [22] C. Frugiuele, J. Pérez-Ríos and C. Peset, *Current and future perspectives of positronium and muonium spectroscopy as dark sectors probe*, *Phys. Rev. D* **100** (2019) 015010 [[1902.08585](#)].
- [23] B. Holdom, *Two $U(1)$'s and Epsilon Charge Shifts*, *Phys. Lett.* **166B** (1986) 196.
- [24] G.F. Giudice, P. Paradisi and M. Passera, *Testing new physics with the electron $g-2$* , *JHEP* **11** (2012) 113 [[1208.6583](#)].
- [25] S.G. Karshenboim, D. McKeen and M. Pospelov, *Constraints on muon-specific dark forces*, *Phys. Rev. D* **90** (2014) 073004 [[1401.6154](#)].

- [26] I. Beltrami, B. Aas, W. Beer, G. De Chambrier, P. Goudsmit, T. Ledebur et al., *New precision measurements of the muonic $3d5/2 \rightarrow 2p3/2$ x-ray transition in 24Mg and 28Si : Vacuum polarisation test and search for muon-hadron interactions beyond qed*, *Nuclear Physics A* **451** (1986) 679.
- [27] C. Peset, A. Pineda and O. Tomalak, *The proton radius (puzzle?) and its relatives*, [2106.00695](#).
- [28] R. Pohl et al., *The size of the proton*, *Nature* **466** (2010) 213.
- [29] A. Antognini et al., *Proton Structure from the Measurement of $2S - 2P$ Transition Frequencies of Muonic Hydrogen*, *Science* **339** (2013) 417.
- [30] H. Fleurbaey, S. Galtier, S. Thomas, M. Bonnaud, L. Julien, F. Biraben et al., *New Measurement of the $1S - 3S$ Transition Frequency of Hydrogen: Contribution to the Proton Charge Radius Puzzle*, *Phys. Rev. Lett.* **120** (2018) 183001 [[1801.08816](#)].
- [31] A. Grinin, A. Matveev, D.C. Yost, L. Maisenbacher, V. Wirthl, R. Pohl et al., *Two-photon frequency comb spectroscopy of atomic hydrogen*, *Science* **370** (2020) 1061 [<https://science.sciencemag.org/content/370/6520/1061.full.pdf>].
- [32] A. Beyer et al., *The Rydberg constant and proton size from atomic hydrogen*, *Science* **358** (2017) 79.
- [33] CREMA collaboration, *Laser spectroscopy of muonic deuterium*, *Science* **353** (2016) 669.
- [34] J.J. Krauth et al., *Measuring the α -particle charge radius with muonic helium-4 ions*, *Nature* **589** (2021) 527.
- [35] R.P. talk, *Nucleon and nuclear structure from measurements in muonic and normal atoms*, <https://pa.as.uky.edu/tba-98>.
- [36] M. Horbatsch and E.A. Hessels, *Tabulation of the bound-state energies of atomic hydrogen*, *Phys. Rev. A* **93** (2016) 022513.
- [37] J.J. Krauth, M. Diepold, B. Franke, A. Antognini, F. Kottmann and R. Pohl, *Theory of the $n=2$ levels in muonic deuterium*, *Annals Phys.* **366** (2016) 168 [[1506.01298](#)].
- [38] C.G. Parthey, A. Matveev, J. Alnis, R. Pohl, T. Udem, U.D. Jentschura et al., *Precision Measurement of the Hydrogen-Deuterium $1S$ - $2S$ Isotope Shift*, *Phys. Rev. Lett.* **104** (2010) 233001.
- [39] C.G. Parthey et al., *Improved Measurement of the Hydrogen $1S - 2S$ Transition Frequency*, *Phys. Rev. Lett.* **107** (2011) 203001 [[1107.3101](#)].
- [40] K. Pachucki, V.c.v. Patkóš and V.A. Yerokhin, *Three-photon-exchange nuclear structure correction in hydrogenic systems*, *Phys. Rev. A* **97** (2018) 062511.
- [41] O.J. Hernandez, A. Ekström, N. Nevo Dinur, C. Ji, S. Bacca and N. Barnea, *The deuteron-radius puzzle is alive: A new analysis of nuclear structure uncertainties*, *Phys. Lett. B* **778** (2018) 377 [[1711.01199](#)].
- [42] B. Acharya, V. Lensky, S. Bacca, M. Gorchtein and M. Vanderhaeghen, *Dispersive evaluation of the Lamb shift in muonic deuterium from chiral effective field theory*, *Phys. Rev. C* **103** (2021) 024001 [[2010.11155](#)].
- [43] M. Diepold, B. Franke, J.J. Krauth, A. Antognini, F. Kottmann and R. Pohl, *Theory of the Lamb shift and Fine Structure in muonic ^4He ions and the muonic $^3\text{He} - ^4\text{He}$ Isotope Shift*, *Annals Phys.* **396** (2018) 220 [[1606.05231](#)].

- [44] I. Sick, *Precise root-mean-square radius of He-4*, *Phys. Rev. C* **77** (2008) 041302.
- [45] J.J. Krauth, L.S. Dreissen, C. Roth, E.L. Gründeman, M. Collombon, M. Favier et al., *Paving the way for fundamental physics tests with singly-ionized helium*, *Proceedings of International Conference on Precision Physics and Fundamental Physical Constants ,Äi PoS(FFK2019)* (2019) .
- [46] M. Herrmann, M. Haas, U.D. Jentschura, F. Kottmann, D. Leibfried, G. Saathoff et al., *Feasibility of coherent xuv spectroscopy on the 1s–2s transition in singly ionized helium*, *Phys. Rev. A* **79** (2009) 052505.
- [47] M. Kalinowski, K. Pachucki and V.A. Yerokhin, *Nuclear-structure corrections to the hyperfine splitting in muonic deuterium*, *Phys. Rev. A* **98** (2018) 062513 [1810.06601].
- [48] S.G. Karshenboim, *Precision physics of simple atoms: QED tests, nuclear structure and fundamental constants*, *Phys. Rept.* **422** (2005) 1 [hep-ph/0509010].
- [49] U.D. Jentschura and V.A. Yerokhin, *Quantum electrodynamic corrections to the hyperfine structure of excited s states*, *Phys. Rev. A* **73** (2006) 062503.
- [50] N. Kolachevsky, A. Matveev, J. Alnis, C.G. Parthey, S.G. Karshenboim and T.W. Hänsch, *Measurement of the 2s hyperfine interval in atomic hydrogen*, *Phys. Rev. Lett.* **102** (2009) 213002.
- [51] C. Peset and A. Pineda, *Model-independent determination of the two-photon exchange contribution to hyperfine splitting in muonic hydrogen*, *JHEP* **04** (2017) 060 [1612.05206].
- [52] A. Adamczak, D. Bakalov, L. Stoychev and A. Vacchi, *Hyperfine spectroscopy of muonic hydrogen and the PSI Lamb shift experiment*, *Nucl. Instrum. Meth. B* **281** (2012) 72.
- [53] FAMU collaboration, *Steps towards the hyperfine splitting measurement of the muonic hydrogen ground state: pulsed muon beam and detection system characterization*, *JINST* **11** (2016) P05007 [1604.01572].
- [54] S. Schmidt et al., *The next generation of laser spectroscopy experiments using light muonic atoms*, *J. Phys. Conf. Ser.* **1138** (2018) 012010 [1808.07240].
- [55] D. Croon, G. Elor, R.K. Leane and S.D. McDermott, *Supernova Muons: New Constraints on Z' Bosons, Axions and ALPs*, *JHEP* **01** (2021) 107 [2006.13942].
- [56] H. Leeb and J. Schmiedmayer, *Constraint on hypothetical light interacting bosons from low-energy neutron experiments*, *Phys. Rev. Lett.* **68** (1992) 1472.
- [57] MUON $g - 2$ COLLABORATION collaboration, *Measurement of the positive muon anomalous magnetic moment to 0.46 ppm*, *Phys. Rev. Lett.* **126** (2021) 141801.
- [58] J. Kozaczuk, D.E. Morrissey and S.R. Stroberg, *Light axial vector bosons, nuclear transitions, and the ^8Be anomaly*, *Phys. Rev. D* **95** (2017) 115024 [1612.01525].
- [59] S.G. Karshenboim, *Constraints on a long-range spin-dependent interaction from precision atomic physics*, *Phys. Rev. D* **82** (2010) 113013 [1005.4868].
- [60] A. Ringwald, *Axions and Axion-Like Particles*, in *49th Rencontres de Moriond on Electroweak Interactions and Unified Theories*, 7, 2014 [1407.0546].
- [61] K. Choi, S.H. Im and C.S. Shin, *Recent progress in physics of axions or axion-like particles*, [2012.05029](#).

- [62] B.C. Odom, D. Hanneke, B. D’Urso and G. Gabrielse, *New Measurement of the Electron Magnetic Moment Using a One-Electron Quantum Cyclotron*, *Phys. Rev. Lett.* **97** (2006) 030801.
- [63] D. Hanneke, S. Fogwell and G. Gabrielse, *New measurement of the electron magnetic moment and the fine structure constant*, *Physical Review Letters* **100** (2008) .
- [64] ACME collaboration, *Order of Magnitude Smaller Limit on the Electric Dipole Moment of the Electron*, *Science* **343** (2014) 269 [[1310.7534](#)].
- [65] W.E. Caswell and G.P. Lepage, *Effective Lagrangians for Bound State Problems in QED, QCD, and Other Field Theories*, *Phys. Lett.* **167B** (1986) 437.
- [66] A. Pineda, *Review of Heavy Quarkonium at weak coupling*, *Prog. Part. Nucl. Phys.* **67** (2012) 735 [[1111.0165](#)].
- [67] M. Beneke, Y. Kiyo and K. Schuller, *Third-order correction to top-quark pair production near threshold I. Effective theory set-up and matching coefficients*, [1312.4791](#).
- [68] N. Brambilla, H.S. Chung, V. Shtabovenko and A. Vairo, *FeynOnium: Using FeynCalc for automatic calculations in Nonrelativistic Effective Field Theories*, *JHEP* **11** (2020) 130 [[2006.15451](#)].
- [69] A. Pineda and J. Soto, *Matching at one loop for the four quark operators in NRQCD*, *Phys. Rev. D* **58** (1998) 114011 [[hep-ph/9802365](#)].
- [70] N. Brambilla, A. Pineda, J. Soto and A. Vairo, *Potential NRQCD: An Effective theory for heavy quarkonium*, *Nucl. Phys. B* **566** (2000) 275 [[hep-ph/9907240](#)].
- [71] C. Peset, A. Pineda and M. Stahlhofen, *Potential NRQCD for unequal masses and the B_c spectrum at N^3LO* , *JHEP* **05** (2016) 017 [[1511.08210](#)].
- [72] P. Fadeev, Y.V. Stadnik, F. Ficek, M.G. Kozlov, V.V. Flambaum and D. Budker, *Revisiting spin-dependent forces mediated by new bosons: Potentials in the coordinate-space representation for macroscopic- and atomic-scale experiments*, *Phys. Rev. A* **99** (2019) 022113 [[1810.10364](#)].
- [73] Y. Kiyo and Y. Sumino, *Full Formula for Heavy Quarkonium Energy Levels at Next-to-next-to-next-to-leading Order*, *Nucl. Phys. B* **889** (2014) 156 [[1408.5590](#)].